JfM PAPERS

A semi-empirical model to predict resonant conditions in valveless asymmetric pumping

M. Rubio[1] (ORCID)**, J. Anatol**[1]**, J. Sierra-Pallares**[1]**, C. Barrios-Collado**[1] **and F. Castro-Ruiz**[1]

[1]Depto. de Ingeniería Energética y Fluidomecánica and Instituto de las Tecnologías Avanzadas de la Producción (ITAP), Universidad de Valladolid, E-47003 Valladolid, Spain

Corresponding author: M. Rubio, manuel.rubio@uva.es

The Liebau effect generates a net flow without the need for valves. For the Liebau effect pumping phenomenon to occur, the pump must have specific characteristics. It needs tubes with different elastic properties and an actuator to provide energy to the fluid. The actuator periodically compresses the more flexible element. Furthermore, asymmetry is a crucial factor that differentiates between two pumping mechanisms: impedance pumping and asymmetric pumping. In this work, a model based on the fluid dynamics of an asymmetric valveless pump under resonant conditions is proposed to determine which parameters influence the pumped flow rate. Experimental work is used to validate the model, after which each of the parameters involved in the pump performance is dimensionlessly analysed. This highlights the most significant parameters influencing the pump performance such as the actuator period, length tube ratio and tube diameters. The results point out ways to increase a valveless asymmetric pump's net-propelled flow rate, which has exciting applications in fields such as biomedicine. The model also allows for predicting the resonance period, a fundamental operating parameter for asymmetric pumping.

Key words: propulsion, peristaltic pumping

1. Introduction

The Liebau effect (Liebau 1954) creates a net flow without the use of valves. The instantaneous pumped flow rate is bidirectional and pulsatile (Davtyan & Sarvazyan 2021). For the phenomenon to take place, the pump needs to have particular characteristics:

tubes of different mechanical properties (commonly a flexible and a rigid tube), a periodic compression of the flexible element by an actuator and a condition of asymmetry either in the pincher with respect to the flexible tube or in the circuit (Moser 1998; Kenner *et al.* 2000; Kenner 2004; Anatol *et al.* 2022, 2024). Liebau effect pumps are simple pumping devices. This feature makes them very suitable for integration when a non-invasive, space-saving pumping system is required (Propst 2006). For these reasons, valveless pumping with Liebau effect pumps is especially interesting for applications in nanotechnology (Andersson *et al.* 2001), chemical analysis and control (Wen *et al.* 2006), microengineering (Lee, Chang & Wen 2008), cooling systems (Wen *et al.* 2013), and in biomedical engineering. In the latter field, Liebau-effect pumps are a good choice as they work with small excitations, a condition that may be necessary in confined environments (Loumes, Avrahami & Gharib 2008).

Asymmetry is a crucial factor that allows for the differentiation between two pumping mechanisms: impedance pumping and asymmetric pumping (Pahlevan & Gharib 2013). Depending on the mechanism generating the pumping, three types of pumps can be distinguished: impedance pumps, asymmetric pumps and Liebau pumps, the latter combining the two mechanisms. Without any asymmetry, no pumping effect occurs and no net flow is generated, underscoring the significance of this condition (Hickerson 2005; Wen & Chang 2009; Hiermeier & Männer 2017; Manopoulos, Tsangaris & Mathioulakis 2020; Davtyan & Sarvazyan 2021).

Impedance pumping occurs when the flexible tube's compression occurs outside its plane of symmetry. The flexible tube is connected to a rigid pipe at both ends, so the circuit has a significant impedance difference at these points. Impedance can be defined as the resistance imposed by a medium to a wave propagating through it (Wen & Chang 2009). The pumping cycle starts with the compression of the flexible tube. As it is compressed, mechanical energy is added to the fluid, mainly in the form of pressure, generating bidirectional waves that travel from the point of compression to the ends of the flexible tube, where they are partially reflected due to the change in impedance at the junction with the stiffer tube (Hickerson, Rinderknecht & Gharib 2005). The interaction of the emitted and reflected waves can result in a net unidirectional flow (Loumes *et al.* 2008; Avrahami & Gharib 2008; Wen & Chang 2009; Wen *et al.* 2013).

Asymmetric pumping occurs when the compression of the flexible tube is in its plane of symmetry, but there is an asymmetry in the adjacent circuit. The asymmetry may be due to the difference in length, diameter or material of the rigid tubes. Kenner *et al.* (2000); Kenner (2004) discussed this asymmetry regarding inertia and energy losses.

Finally, the so-called Liebau pump corresponds to mixed pumping as it combines the two mechanisms: impedance pumping and asymmetric pumping. There is double asymmetry: the flexible tube is compressed outside its plane of symmetry and the circuit is asymmetric. The right combination of both effects has increased performance (Wen & Chang 2009; Pahlevan & Gharib 2013).

The impedance pumping mechanism has been studied experimentally (Moser 1998; Hickerson *et al.* 2005; Bringley *et al.* 2008; Wen *et al.* 2013; Manopoulos *et al.* 2020; Davtyan & Sarvazyan 2021), and by numerical and analytical models (Hickerson & Gharib 2006; Bringley *et al.* 2008; Loumes *et al.* 2008; Avrahami & Gharib 2008). However, there are fewer experimental (Takagi 1983,1985; Anatol *et al.* 2022, 2023, 2024) and numerical (Takagi 1983,1985; Propst 2006; Jung & Kim 2012) works related to asymmetric pumping. The most well-known models presented to date for asymmetric pumping are presented below.

Takagi (1983) analysed analytically and experimentally the behaviour of an asymmetric pump in a circuit consisting of a horizontal pipe connecting two tanks and a piston

operating in a T-junction that divides the pipe into two sections. The piston was located in a non-equidistant location from both tanks. They developed a mathematical model from the equations of continuity and quantity of motion that could predict the pumping effect, which agreed with the experimental data. Takagi (1985) continued this work. They observed that the pumping effect increases with the difference between the velocity amplitudes in each horizontal pipe section. Finally, they obtained information on the resonant frequency and found that the pump performance was higher at this frequency.

Propst (2006) described numerically the theoretical foundations of asymmetric pumping using the time-averaged energy equation. He considered different circuit configurations consisting of tanks connected by rigid pipes. From his analysis, he deduced that pumping is caused by the difference in kinetic energy between the two pipe sections and that the difference in tank levels is proportional to the difference in kinetic energy between the two branches. The magnitude of the net flux generated increases with the degree of asymmetry.

Jung & Kim (2012) proposed a mathematical model of an asymmetric valveless pump consisting of two tanks connected with a horizontal pipe. They used an energy conservation model applied to consecutive control volumes, which they called compartments, in one or more of which the mechanical actuation on a piece of pipe could be modelled. They confirmed that the direction and magnitude of the net flow depend on the compression frequency and confirmed that the resonant frequency is the optimal frequency for working with asymmetric pumps. At this frequency, time-phase synchronisation is obtained between the fluid pressure difference and the external compression force, allowing energy storage in the discharge tank.

In the two works by Takagi and the one by Propst, pumps with a similar set-up of elements to that presented in this paper have been analysed, although they do not have the flexible pipe typical of Liebau pumps. Regarding Jung's work, a model with an identical distribution of elements to that employed in this study has been developed, although validation is lacking. To our knowledge, there is little work published in the open literature regarding validation of mathematical models of asymmetric pumping.

This work proposes a semiempirical model using continuity and momentum equations to describe the flow mechanism of an asymmetric valveless pump under resonant conditions. The resonant conditions are those in which the flow rate is maximised, so this is the operating point at which the pump must work. This model allows to determine which parameters influence the pumped flow rate. Experimental work by Anatol *et al.* (2023) is used to validate the model, after which each of the parameters involved in the pump performance is analysed dimensionlessly. The work is structured as follows: in § 2, on materials and methods, the test rig is described and the flow equations are detailed. After that, the pumping mechanism, the model used and the utmost flow rate the pump could provide under ideal conditions are explained. Section 3, on discussion, is divided into two main parts, the validation and the parametric study. In the validation part, experiments under resonant conditions for different test rig geometries are used to validate the model. Once the model is validated, the parametric study analyses the effect of both geometrical and operational parameters. In addition, the parametric study proposes an adimensionalisation that highlights the parameters influencing the pump performance.

2. Materials and methods

2.1. *Experimental test rig*

The experimental set-up will be the same as that of Anatol *et al.* (2023). Figure 1 shows the geometrical parameters taken into account in the analysis carried out in this paper. From now on, the flexible tube will be called a compliant tube and the actuator will be called
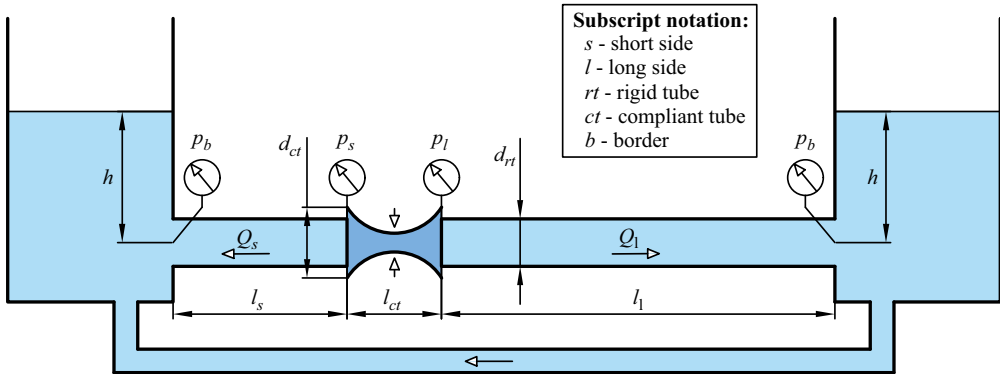
Figure 1. Experimental test rig of Anatol *et al.* (2023). The nomenclature of this work is different from that used in that paper.

a pincher. The experimental set-up comprises six parts: the short-side tank, short rigid pipe, compliant tube, long rigid pipe, long-side tank and return pipe connecting the two tanks. To facilitate the follow-up of the work, the nomenclature has been modified from that of Anatol *et al.* (2023). In addition, the flow rates will be positive in this work when leaving the compliant tube, as shown in figure 1. In the discussion section, the values of the dimensions and operating conditions tested will be given. The working fluid is water.

2.2. *Equations*

We start from the Navier–Stokes equations for incompressible flow:

$$\boldsymbol{\nabla} \cdot \boldsymbol{v} = 0, \tag{2.1}$$

$$\rho \frac{\mathrm{D}\boldsymbol{v}}{\mathrm{D}t} + \boldsymbol{\nabla} p = \mu \boldsymbol{\Delta} \boldsymbol{v} + \rho \boldsymbol{f_m}. \tag{2.2}$$

In the present work, we will apply the above equations to the asymmetric pump's short and long pipes. A cylindrical coordinate system will be used, where z is axial to the pipes. If it is particularised for the horizontal pipes (so $\boldsymbol{f_m} = 0$) and unidirectional flow is assumed (then, $\boldsymbol{v} \approx v_z \boldsymbol{e_z}$), we obtain

$$\rho \frac{\partial v_z}{\partial t} + \frac{\partial p}{\partial z} \approx \mu \left(\frac{\partial^2 v_z}{\partial r^2} + \frac{1}{r} \frac{\partial v_z}{\partial r} \right). \tag{2.3}$$

The axial pressure gradient can be calculated from the pressure difference between the ends of each pipe, $\Delta p = p_{ct} - p_b$, and their respective length, l. Here, p_{ct} is the pressure in the compliant tube and p_b is the hydrostatic pressure at the edge of the pipe. Therefore, $\partial p / \partial z = -\Delta p / l$, where the negative sign is introduced for convenience.

Concerning the effect of viscosity, if we assume it plays a negligible role, this implies that the order of the transient term in (2.3) is dominant over the term associated with viscous stresses. This will be verified through an order of magnitude analysis of these terms in a rigid pipe. If the transient term dominates over that associated with viscous stresses, it implies that $\rho (v_c/t_c) \gg \mu (v_c/d_{rt}^2)$, where t_c and v_c are the characteristic time and velocity in the rigid pipes, and d_{rt} is the diameter of those pipes. With these two terms, the Womersley number (Wo) is obtained, which must be much greater than 1 to disregard the effect of viscosity,

$$Wo^2 = \frac{\rho/t_c}{\mu/d_{rt}^2} \gg 1. \tag{2.4}$$

To calculate this number, it is necessary to determine the characteristic time. If the order of the transient term is equated with that of the term associated with pressures, it is obtained that $\rho(v_c/t_c) \sim \Delta p/l$. If $v_c \approx l/t_c$ and $\Delta p \approx p_b$, then $t_c \sim (\rho l^2/p_b)^{1/2}$. In the experiments analysed in this work, with the dimensions detailed in § 3, Wo^2 is always greater than 100, which allows us to eliminate the term associated with viscous stresses from (2.3). If this term were not removed from the equation, the model presented in this work could be resolved by considering the velocity profiles defined by Womersley (1955) in his study on pulsatile laminar flow.

It is convenient to rewrite the above equation in terms of flow rate by the simple expression $Q = v_z A_{rt}$, where A_{rt} is the cross-sectional area of the rigid pipes $A_{rt} = \pi d_{rt}^2/4$. With the above assumptions, we arrive at

$$\frac{\rho l}{A_{rt}} \frac{\partial Q}{\partial t} = \Delta p. \tag{2.5}$$

Finally, it is helpful to have an expression that relates the volume flowing through the pipe cross-section as a function of time. This can be calculated from expression (2.5) using the definition $Q = dV/dt$. This leads to

$$\frac{\rho l}{A_{rt}} \frac{\partial^2 V}{\partial t^2} = \Delta p. \tag{2.6}$$

2.3. *Pumping cycle under resonant conditions*

Resonant conditions are those at which the flow rate is maximised (Takagi 1985). Experimentally, it has been observed that these conditions occur when the volume in the tube that varies as shown in figure 2(*a*). This section will deal with the analytical procedure to obtain the resonant period and the theoretical flow rate that the pump provides under these conditions. To do this, at first, we describe the pumping mechanism and then the mathematical model used.

2.3.1. *Pumping mechanism*

The pumping mechanism is elucidated using the cycle detailed by Anatol *et al.* (2023), depicted in figure 2(*b–d*). This cycle occurs under resonance conditions. To enable readers to closely observe the evolution of the compliant tube under these conditions, a slow-motion video has been included in the supplementary material of the paper. The video experiment employs the same set-up as Anatol *et al.* (2023), with the exception that the pincher has been replaced by a mechanical one. To further clarify the pumping mechanism, the most significant moments of the cycle have been selected and illustrated in figure 2(*a*).

The beginning of the cycle (instant t_1 figure 2*a*) comes when the compliant tube has its maximum volume, $V_{ct,1}$ (figure 2*d*). This instant coincides experimentally when the short-side flow rate, Q_s, is almost zero (figure 2*c*). As the volume of the compliant tube is greater than at rest, the walls are stretched and exert an overpressure on the fluid. This overpressure causes the pressure in the compliant tube to be higher than in the tanks (figure 2*b*). Moreover, under resonance conditions, the actuator pinches the compliant tube just after this moment, further stretching the walls. From this moment on, if the pincher is positioned in the centre of the compliant tube, it displaces half of the volume on each side of the compliant tube (Kenner *et al.* 2000). If we allow time to elapse, the outflow on the short side increases as a result of the pressure difference between the compliant tube and the tank, as shown in (2.5)), where $\Delta p_s = p_s - p_b$ is positive. This flow rate causes the volume of the compliant tube to decay.
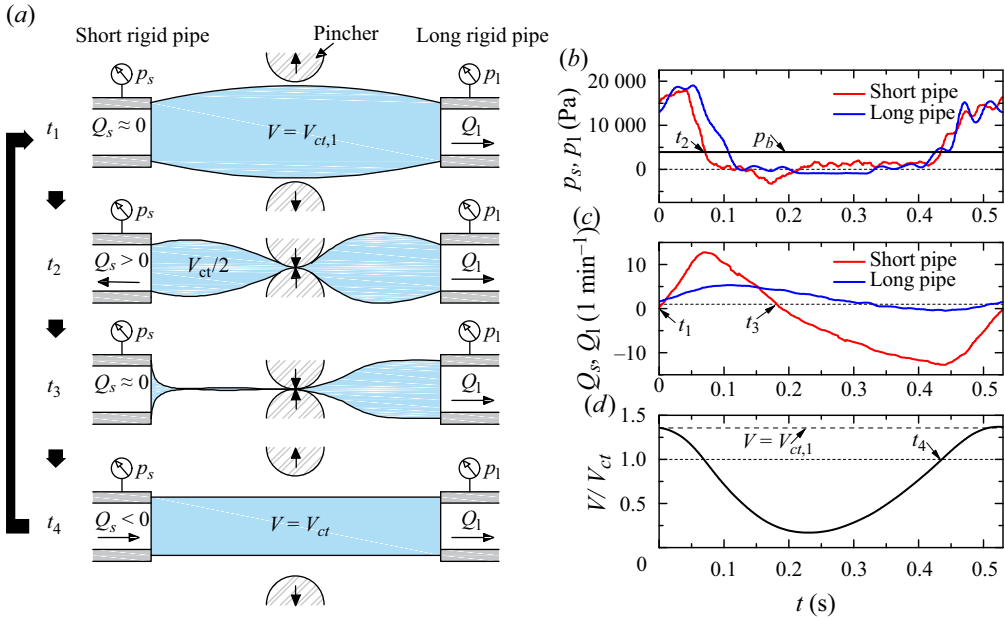
Figure 2. (*a*) Schematic representation of stages of a pumping cycle in resonant conditions. (*b*) Gauge pressure on the short-side p_s (red line) and long-side p_l (blue line); (*c*) flow rate on the short-side Q_s (red line) and long-side Q_l (blue line) and (*d*) volume of the compliant tube dimensioned V/V_{ct} as a function of time over one cycle. The experiment is from Anatol *et al.* (2023).

The instant t_2 is marked by the moment when the pressure in the short-side half of the compliant tube is equalised with the pressure in the tanks. This approximately coincides when the volume of the short-side compliant tube is half the volume of the compliant tube at rest, $V_{ct}/2$. This volume can be calculated using the formula $V_{ct} = l_{ct}\pi d_{ct}^2/4$. From t_2 onwards, the pressure in the short-side compliant tube half, p_s, falls below that of the tank, even to negative values. Because of this, the pressure difference between the compliant tube and the tank Δp_s is negative, and the outlet flow rate decreases.

On the long side, the same process happens, as explained so far, but with a lower flow rate. Analytically, an explanation can be given from (2.5) considering the level of the two tanks to be similar. If it is also considered a uniform pressure throughout the compliant tube, Δp will be the same for both pipes. By analysing the order of the transient term of (2.5), we arrive at the expression (2.7), where it is observed that the flow rate on the short side will be higher than on the long side with a relationship marked by the proportion between the lengths of the pipes. From now on, this relationship will be called λ. The parameter λ should be high, as seen in § 3, so the flow rate on the long side will be of a lower magnitude than on the short side,

$$\frac{Q_s}{Q_l} \approx \frac{l_l}{l_s} = \lambda. \tag{2.7}$$

The moment at which the flow rate on the short side returns to zero marks the instant t_3. In that instant, the volume in the short-side compliant tube half is almost zero. The pressure in this half is still lower than the pressure in the tank (negative Δp_s), which causes fluid to enter the compliant tube from the short side. From this point on, the pincher must be removed so that it does not prevent the filling of the compliant tube from the short side. Sometime after t_3, the flow rate into the short side will exceed the flow out of the long

side, and the compliant tube will start to fill again. In figure 2(*c*), this happens at 0.22 s, where $V/V_{ct} \approx 0.2$.

The last instant of the cycle, t_4, is marked by the moment at which the pressure in the compliant tube becomes equal again to the pressure in the tanks. It approximately coincides when the total volume of the compliant tube is the rest volume, V_{ct}. It means that the walls of the compliant tube are not stretched. After this, it will be stretched again and the pressure exerted by the compliant tube will be higher than the pressure in the tanks. Once its maximum volume is reached, the cycle will repeat.

Between the instant t_1 and t_3, half of the volume $V_{ct,1}$ has been expelled from the short side. While this is happening, a volume of less than half has been emptied from the long side due to its lower flow rate, according to the ratio (2.7). The rest of the time, the compliant tube is filled with fluid from the short side with a volume more significant than that expelled from the short side between t_1 and t_3. This excess volume on the short side (or shortfall on the long side) is the cause of the net flow from the short to the long side.

2.3.2. *Model*

Having described the pumping mechanism under resonant conditions, the volumes and flow rates described above will be used to develop a model to predict the pump's behaviour. The model is sensitive to the set-up, and parameters both upstream and downstream are needed for obtaining a prediction. The significant assumption of the model is that there are only two possible values of pressures inside the compliant tube: p_m when the compliant tube has an excess volume concerning its volume at rest, V_{ct}; and zero gauge pressure when the volume of the compliant tube is less than V_{ct}. In this work, the pressure at the ends of the rigid tubes in contact with the tank, p_b, it does not vary throughout the cycle. This has been chosen to replicate the conditions of the experiments conducted by Anatol *et al.* (2023); however, a generic pressure could be used.

The dimensions of the test rig $l_s, l_l, l_{ct}, d_{ct}, d_{rt}$ are assumed to be known. Here, V_{ct} can be calculated from these dimensions, but not its maximum volume, $V_{ct,1}$. This volume is essential for the model. For its calculation, the short side will be analysed when the pincher is acting, which causes the compliant tube to split into two independent parts.

For obtaining $V_{ct,1}$, the expressions to calculate the short pipe instantaneous flow rate (Q_s) at a certain time t and dispaced volume ($V_{s,if}$) between two instants (t_i and t_f) are introduced. Here, Q_s is obtained by integrating (2.8) between the initial instant t_i and an arbitrary t:

$$\frac{\partial Q_s}{\partial t} = \Delta p_s \frac{A_{rt}}{\rho l_s} \implies \int_{Q_{s,i}}^{Q_s} dQ_s = \int_{t_i}^{t} \frac{\Delta p_s A_{rt}}{\rho l_s} dt \implies Q_s = Q_{s,i} + \frac{\Delta p_s A_{rt}}{\rho l_s}(t - t_i). \tag{2.8}$$

Thus, $V_{s,if}$ could be obtained by the following expression:

$$\frac{\partial V_s}{\partial t} = Q_s \implies \int_{V_{s,i}}^{V_{s,f}} dV_s = \int_{t_i}^{t_f} Q_s dt \implies$$

$$\implies V_{s,if} = V_{s,f} - V_{s,i} = \frac{\Delta p_s A_{rt}}{\rho l_s} \frac{(t_f - t_i)^2}{2} + Q_{s,i}(t_f - t_i). \tag{2.9}$$

For obtaining the volume $V_{ct,1}$, the time interval $\Delta t_{2,3} = t_3 - t_2$ must be computed. Between instant t_2 and t_3, it is known that half of the short-side compliant tube has lost a volume of $V_{ct}/2$ (figure 2*a*), so the volume flowing through the pipe cross-section will be $V_{s,23} = V_{ct}/2$ by using (2.9). If t_i is t_3 and t_f is t_2, it is possible to know $\Delta t_{2,3}$ assuming

that the pressure in the compliant tube is approximately zero (figure 2c) and, therefore, $\Delta p_s = -p_b = -\rho g h$. At t_3, the flow rate in the short pipe is almost zero ($Q_{s,3} = 0$), and between t_3 to t_2, the ejected volume is $V_{s,32} = -V_{s,23} = -V_{ct}/2$. This leads to the following expression:

$$V_{s,32} = -\frac{V_{ct}}{2} = -\frac{gh A_{rt}}{l_s}\frac{(t_2 - t_3)^2}{2} \implies \Delta t_{2,3} = \sqrt{\frac{V_{ct}l_s}{gh A_{rt}}}. \tag{2.10}$$

Once this time interval is known, it is possible to calculate the flow rate on the short side at instant t_2, $Q_{s,2}$, from (2.8), obtaining $Q_{s,2} = A_{rt}gh\Delta t_{2,3}/l_s$. With this flow rate and that at the instant t_1 (which is zero on the short side), we can calculate the time between instant t_1 and t_2 ($\Delta t_{1,2}$) from (2.8), assuming that the pressure in the compliant tube will be of constant value p_m, due to between t_1 and t_2, the compliant tube is stretched. As indicated, keeping this pressure constant is the significant assumption introduced in the model. In reality, the pressure in the compliant tube is neither uniform nor constant, and depends on its shape and the action of the pincher. To calculate its shape, a fluid–structure simulation or experiments of at least the compliant tube part is necessary, which is not done in this paper. This value of pressure could be related to the instantaneous volume of each compliant tube half and the elastic properties of the material. If this were achieved, the problem could be closed, moving it away from being semi-empirical.

The pressure p_m will be essential in the model since, together with the level of the tanks, they are the only parameters that depend on the operating conditions and not on the dimensions of the test rig. Therefore, between instant t_1 and t_2, the pressure difference between both ends of the short rigid pipe will then be $\Delta p_s = p_s - p_b = p_m - \rho g h$. So the time between both instants is calculated with the expression:

$$Q_{s,2} = \frac{(p_m - \rho g h) A_{rt}}{\rho l_s}(t_2 - t_1) \implies \Delta t_{1,2} = \frac{Q_{s,2}\rho l_s}{A_{rt}(p_m - \rho g h)}. \tag{2.11}$$

After this, $V_{ct,1}$ can be calculated from (2.9). This is the result of adding the volume of the static compliant tube and twice the volume that passes through the short side between t_1 and t_2. Assuming these conditions, we arrive at the following expression:

$$V_{ct,1} = V_{ct} + 2V_{s,12} = V_{ct} + \frac{(p_m - \rho g h)A_{rt}}{\rho l_s}(t_2 - t_1)^2 = V_{ct} + Q_{s,2}\Delta t_{1,2}. \tag{2.12}$$

So, the maximum volume of the compliant tube ($V_{ct,1}$) can be computed as a function of the first part of the experimental cycle. Once volume $V_{ct,1}$ is known, the model is based on the integration of (2.5) and (2.6) using a classic Runge–Kutta 4–5 ordinary differential equation (ODE) solver, and the time series of pressure, volume and flow rate can be reconstructed, as seen in figure 3, where the model predictions are compared with the experimental data from Anatol *et al.* (2023). The pressure in the short-side compliant tube half is p_m between t_1 and t_2. In figure 3, t_1 is $t = 0$ s, and t_2 occurs when the fluid volume passing through the short side, V_s, is $(V_{ct,1} - V_{ct})/2$. The same is assumed for half of the long side. Here, p_m in this experiment is calculated with the mean value of the experimental pressure in the compliant tube when it is stretched.

After t_2, the pressure in the compliant tube will be zero, which is also valid for the long side. The maximum volume that can come out of each side is $V_{ct,1}/2$. After this, filling begins on the short side. At this time, there is no physical separation due to the pincher (it has been displaced), so the pressure of the compliant tube is determined by the total volume of it, not of each half. Therefore, when the total volume of the compliant tube has
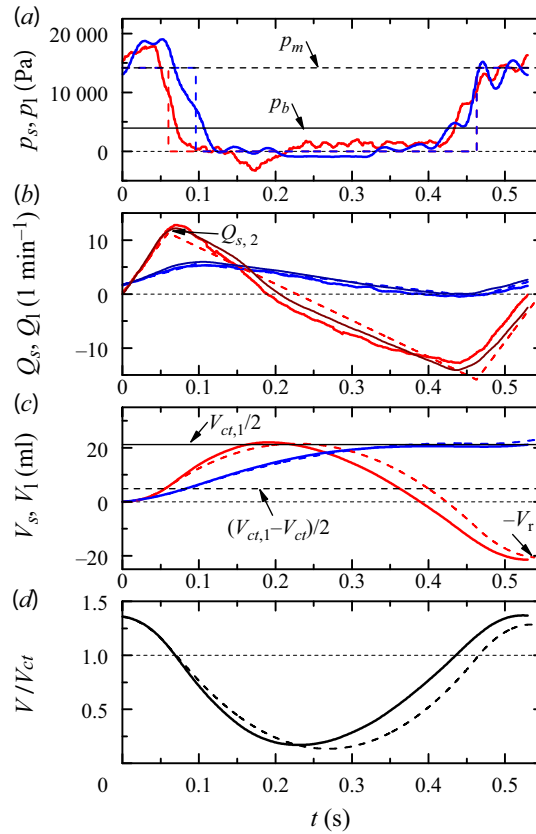
Figure 3. (*a*) Gauge pressure on the short (p_s) and long side (p_l), (*b*) flow rate in the short (Q_s) and long pipe (Q_l), (*c*) volume through the short (V_s) and long side (V_l), and (*d*) total volume of the compliant tube dimensioned with the volume at rest (V/V_{ct}) as a function of time over one cycle. A solid line shows the experimental results and a dashed line shows the model with $p_m = 14\,166\,\text{Pa}$. Red shows the data for the short side, blue for the long side and black for the compliant tube. The dark lines in panel (*b*) represent the integration of (2.5) using the experimental pressure signal. The experiment is from Anatol *et al.* (2023).

values greater than the idle volume, V_{ct}, it is assumed that the pressure in the compliant tube returns to p_m. Finally, the cycle is finished when the derivative of the volume of the compliant tube over time is zero, indicating that it has been refilled. Once the cycle has been finished, the flow rate at resonant conditions, Q_r, is obtained by dividing the negative value of the volume that has passed through the short side at the end of the cycle (V_r in figure 3) and the time at the end of the cycle, T_r, which will be called the resonant period.

Slight differences between the model predictions and the experimental reality are found due to the simple choice of a constant value of p_m for the whole time series. Despite this very simple assumption, the model is able to predict the experimental time series of pressure, volume and flow rate very satisfactorily. Finally, figure 3(*b*) shows that viscosity is subdominant thanks to the integration of (2.5) using the experimental pressure signal to obtain the instantaneous flow rate. As can be seen, there are small differences between the experimental flow rate signal and the integrated one. These differences arise from the integration of an experimental signal, where any lack of precision by the experimental equipment amplifies the error. This comparison definitively validates the assumptions of non-viscous unidirectional flow.

2.3.3. *Pincher duty cycle*

The pincher is necessary to keep the cycle pumping so that the flow rate does not drop due to dissipative effects. However, it should only work in certain parts of the cycle. To be as efficient as possible, it must start to act at instant t_1 and be active at least until instant t_3, to provide enough pressure for half the volume of the compliant tube to go down the short side. However, it must cease exerting pressure before it impairs the flow returning from the short side. It is considered that it must stop exerting pressure before the volume coming from the short side fills half of the compliant tube, and this period coincides with $\Delta t_{2,3}$. Considering all this, the duty cycle range (γ), the percentage of time when the pincher is working, can be obtained with the following expression:

$$\frac{\Delta t_{1,2} + \Delta t_{2,3}}{T_r} \cdot 100 < \gamma < \frac{\Delta t_{1,2} + 2\,\Delta t_{2,3}}{T_r} \cdot 100. \tag{2.13}$$

2.4. *Ideal conditions*

In this section, the utmost flow rate of the pump is going to be calculated using assumptions. The primary assumption is that the flow rate on the long side is assumed to be of a lower order of magnitude than the flow on the short side and is, therefore, not considered in the analysis. As a second assumption, it is considered that $p_m \gg \rho g h$, which implies that $\Delta t_{1,2}$ and $\Delta t_{4,1}$ can be neglected regarding $\Delta t_{2,4}$. Considering the two previous hypotheses, we consider only the short side and the total time of the cycle will be $\Delta t_{2,4}$. The cycle period under these conditions, T_{ic}, will be calculated assuming a pressure difference $\Delta p = -\rho g h$ when the compliant tube is filled, reaching a volume V_{ct}. We will obtain T_{ic} by the integration of (2.5) with the above conditions:

$$T_{ic} = \sqrt{\frac{2\,V_{ct}\,l_s}{A_{rt}\,gh}}. \tag{2.14}$$

In this period, the short-side compliant tube has lost half its volume through the short side and recovered it completely, so the total volume displaced is $V_{ct}/2$. Considering this, the utmost flow rate, Q_{ic}, can be calculated using

$$Q_{ic} = \frac{V_{ct}/2}{T_{ic}} = \sqrt{\frac{V_{ct}\,A_{rt}\,gh}{8\,l_s}}. \tag{2.15}$$

The period and utmost flow rate will be used to adimensionalise the results in the parametric study.

3. Discussion

As indicated, the model set-up is the same as that of Anatol *et al.* (2023). The dimensions involved in the problem are $d_{rt} = 16\,\mathrm{mm}$, $d_{ct} = 20\,\mathrm{mm}$, $l_{ct} = 0.1\,\mathrm{m}$ and $V_{ct} = 31.4\,\mathrm{ml}$. Here, l_s and l_l will vary throughout this section. The model is first validated and then used to perform a parametric sweep.

3.1. *Model validation*

The validation will consist of two stages. First, it will be determined whether the model adequately predicts the resonant period and flow rate. Second, it will be compared with experiments that have varied the test rig's dimensional properties. For both, we will rely on the experiments developed by Anatol *et al.* (2023).
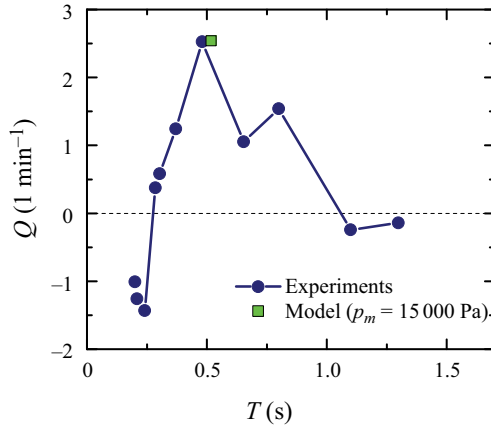
Figure 4. Pumped flow rate (Q) as a function of pincher period (T). The experimental results are shown in blue and the model prediction in green. The dimensions of the pipes are $l_s = 0.7$ m and $l_l = 3.2$ m ($\lambda = 4.57$), and the height of the water column in the tanks, h, is 0.4 m. The experiments are from Anatol *et al.* (2023).
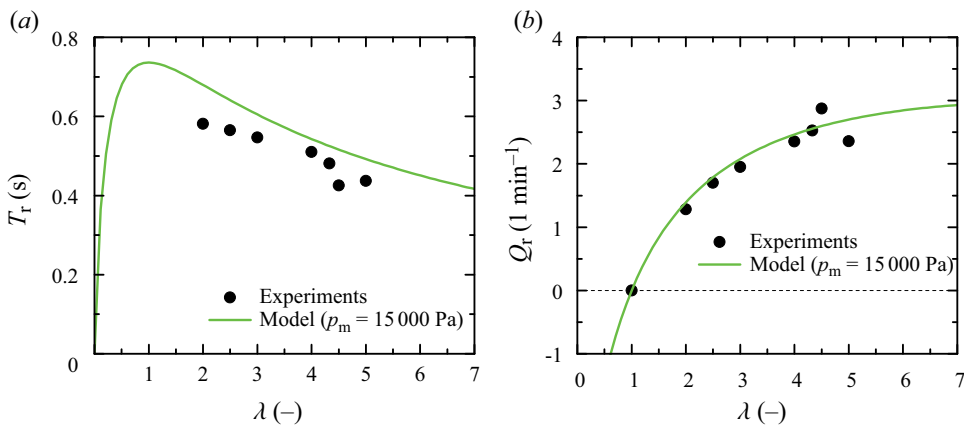

Figure 5. (*a*) Resonant period (T_r) and (*b*) resonant flow rate (Q_r) as a function of the ratio of pipe lengths, λ. The total length of pipes is $l_s + l_l = 4$ m, the pressure p_m is 15 000 Pa and the height of the water column in the tanks, h, is 0.4 m. The experiments are from Anatol *et al.* (2023).

At first, the model will be compared with frequency sweep performed to obtain the flow rate provided by the pump at various periods (figure 4). The dimensions of the pipes are fixed ($l_s = 0.7$ m, $l_l = 3.2$ m). In the figure, it can be seen how the model reliably predicts the resonant flow rate. However, the period is 10 % higher. The reason for this is possibly due to the fact that there are periods when the pressure in the compliant tube drops below 0, a behaviour that is not taken into account by the model (see figure 3*a*). The value of p_m is the average value of the experimental pressure in the compliant tube when it is stretched.

The validation of the model will be continued by comparing it with experiments under resonant conditions. In this step, the length of the short and long pipes is varied, keeping the total length constant, being $l_s + l_l = 4$ m. The ratio of pipe lengths, $\lambda = l_l / l_s$, will be varied obtaining figure 5, where a good correlation between the experiments and the model can be observed. The period obtained by the model remains 10 % higher than the experimental. It can also be seen that the resonant period decreases with λ. The model
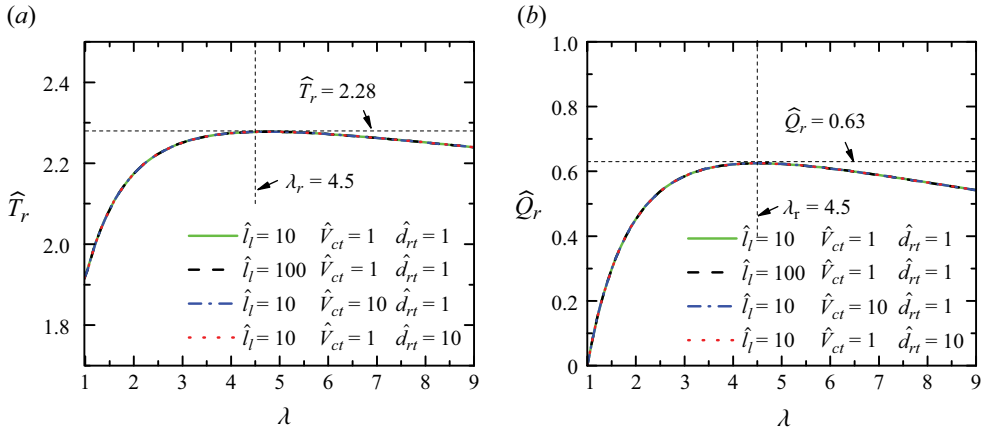
Figure 6. (a) $\widehat{T}_r$ and (b) $\widehat{Q}_r$ as a function of λ for two long span lengths ($\hat{l}_l$), two compliant tube volumes at rest ($\hat{V}_{ct}$), and two different diameters of rigid pipes ($\hat{d}_{rt}$). $\widehat{p}_m$ is 3.8. $\hat{l}_l$ and $\hat{d}_{rt}$ are made dimensionless with $d_{rt} = 16$ mm and $\hat{V}_{ct}$ with $V_{ct} = 31.4$ ml.

shows that a higher λ results in a higher flow rate driven by the pump. After these two steps, the model is considered validated and will be used to perform a parametric sweep.

3.2. *Parametric study*

In this section, the period and flow rate calculated under ideal conditions (§ 2.4) are used to adimensionalise, since they allow interesting conclusions to be drawn. First, we will test the influence of all the dimensions of the test rig involved in the model (l_s, l_l, V_{ct}, d_{rt}). Subsequently, a study is made both of the operating conditions p_m and of the fluid height in the tanks, h.

We begin by analysing the model for different ratios of $\lambda = l_l/l_s$. The λ parameter has been swept for two long pipe lengths, l_l, two compliant tube volumes, V_{ct}, and two rigid pipe diameters, d_{rt}. All this is summarised in figure 6, where the cycle period is adimensionalised with T_{ic}, the net flow rate with Q_{ic} and pressures with $p_b = \rho g h$. The dimensionless parameters will be accented with the caret symbol ($\hat{\ }$). From now on, dimensionless parameters will be used, since they allow interesting conclusions to be drawn. However, the model has been solved dimensionally.

As can be seen in figure 6, all the curves overlap in a curve that has a maximum when $\lambda = \lambda_r = 4.5$. It is in this region where it is of interest for the pump to operate, since the flow rate is maximised. Finally, none of $\hat{l}_l$, $\hat{v}_{ct}$ or $\hat{d}_{rt}$ influence the dimensionless relationships, which results in favour of the proposed dimensionless parameters and allows the problem to be significantly simplified. From the graph, it can be seen that under these operating conditions, to increase the flow rate provided by the pump, there must be a relationship between the lengths of the pipes of $\lambda_r = 4.5$ and Q_{ic} should be as large as possible by increasing V_{ct}, A_{rt} or h, or by decreasing l_s (2.15).

It can be observed that for low λ, the resonant period and flow rate are far from ideal conditions. This is because the hypothesis that the long-side flow rate is of lower order than that on the short side is broken since $Q_s \approx \lambda\, Q_l$ according to (2.7), which explains that for higher λ, this correlation is better.

Finally, the influence of p_m and h is analysed to see how the $\widehat{T}_r$ and $\hat{Q}_r$ ratios change (figure 7). It is obtained for $\lambda_r = 4.5$, as this is the value for which the flow rate obtained in figure 6 is maximised. The abscissa axis represents the dimensionless variable
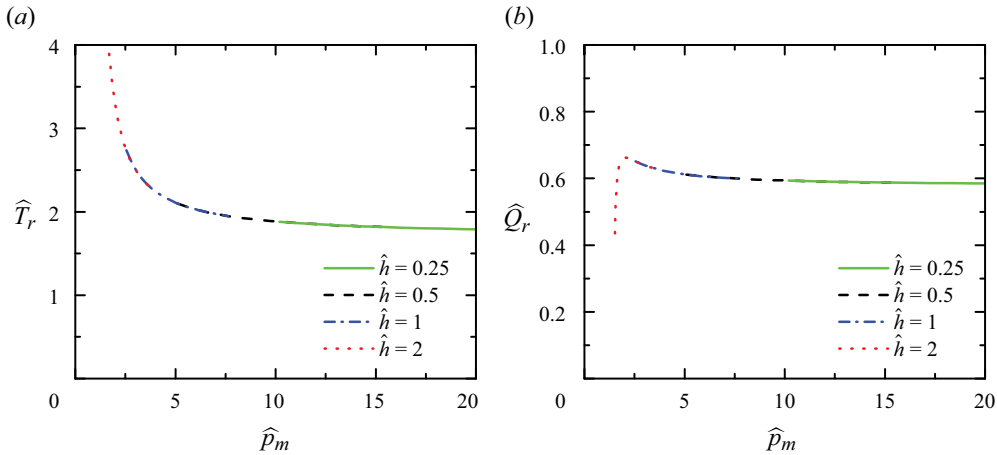
Figure 7. (*a*) $\widehat{T}_r$ and (*b*) $\widehat{Q}_r$ as a function of $\widehat{p}_m$ for several heights of the water column in the tanks, ($\hat{h}$). $\hat{h}$ is made dimensionless with $h = 0.4$ m.

$\widehat{p}_m = p_m / \rho g h$. The model is solved by sweeping p_m for different tank heights. It can be seen how all the curves converge in one that depends only of $\widehat{p}_m$. The value of $\widehat{Q}_r$ is approximately 0.6, except for values of $\widehat{p}_m$ lower than 2. This is a very interesting result because it indicates that the flow rate cannot be increased through this parameter. However, to achieve the indicated $\widehat{Q}_r$, it is necessary for a value of $\widehat{T}_r$ that does depend on $\widehat{p}_m$.

The ratio of pipe lengths, λ, is 4.5.

The unique dependence of the results on the parameters λ and $\widehat{p}_m$ is explained by non-dimensionalising (2.5) using Q_{ic} for the flow rate and T_{ic} for the time for the short and long pipes. If $\Delta p = p_m - \rho g h$, the following equations are obtained:

$$\frac{\partial \hat{Q}_s}{\partial \hat{t}} = 4\,(\widehat{p}_m - 1), \tag{3.1}$$

$$\frac{\partial \hat{Q}_l}{\partial \hat{t}} = 4\,(\widehat{p}_m - 1)\,\frac{1}{\lambda}. \tag{3.2}$$

As can be seen in the equations, the evolution of the dimensionless flow rate in the short and long pipes depends only on these two parameters. Moreover, $\Delta p = p_m - \rho g h$ only occurs when the volume in the compliant tube is greater than the resting volume, which happens only in a small part of the cycle. The duration of this part decreases if the value of $\widehat{p}_m$ increases, having a smaller effect on the net ejected flow rate (figure 7*b*). In this case, for most of the cycle, $\Delta p = -\rho g h$, and the evolution of the dimensionless flow rate will mainly depend only on λ. In this scenario ($\widehat{p}_m >> 1$), the ejected flow rate will depend exclusively on geometric conditions, thereby ceasing the model's semi-empirical nature.

Summarising, for $\widehat{p}_m >> 1$, the chosen adimensionalisation reduces the number of parameters influencing the flow rate to only one, λ, significantly simplifying the problem.

4. Conclusions

This paper explains the pumping mechanism of an asymmetric valveless pump and provides a model for calculating the resonant period and flow rate. The work draws some conclusions. The first one is that the role of viscous dissipation in this type of pumping is subdominant and can be eliminated from the analysis if the Womersley number is high enough.

The pumping mechanism has been described comprehensively. The model has been validated with experiments published by Anatol *et al.* (2023), showing that it acceptably predicts both the resonant period and flow rate. The fundamental role of the ratio between short and long pipe lengths, represented by the parameter $\lambda = l_l\,/\,l_s$, has been determined. The net flow rate under resonant conditions increases with this parameter. However, if the flow rate is adimensioned, as proposed in this work, a maximum is obtained for a particular value of λ, which indicates that to maximise the flow rate, the parameter Q_{ic} must be higher by increasing V_{ct}, A_{rt} or h or decreasing l_s. The model also allows for predicting the resonance period, a fundamental operating parameter for pumping. The proposed adimensionalisation simplifies the problem by reducing the parameters influencing to λ and the ratio $p_m/\rho g h$. In fact, only λ intervenes in the dimensionless flow rate $\widehat{Q}_r$ for $p_m/\rho g h$ higher than 2. The pressure at the ends of the rigid pipes in contact with the tanks, p_b, has been assumed constant through the cycle in this work, but there is no limitation regarding the use of a generic pressure, which would extend its applicability.

The model uses only two pressure values inside the compliant tube, p_m and 0, which is a simplification of reality; to calculate this accurately, fluid–structure simulations or experiments are needed. The dependence of the pressure inside the compliant tube on its volume would be necessary to close the problem. Currently, the parameter is obtained semi-empirically, and therefore, at least one experiment is needed to determine its value. However, in figure 5, it can be observed that the results are acceptable for the geometries studied in this work using a single value of p_m. This may be due to two reasons: either this parameter does not change with geometry or it does not significantly influence the net flow rate. The analysis of this parameter in figure 7 highlights the second option, indicating that p_m has little influence on the net flow rate as long as $p_m/\rho g h$ is greater than 2.

As future work, the analysis of a Liebau pump is proposed, which incorporates both pumping mechanisms: asymmetric and impedance. Furthermore, a fluid–structure simulation will provide a detailed understanding of the pumping dynamics in the compliant tube, helping to understand the influence of the material's elastic properties. Regarding the boundary condition p_b, the model should be generalised by using different pressure conditions. This will enhance understanding of the potential applications of Liebau pumps.

The present work points out ways to understand the asymmetric pumping mechanisms and thus being able to optimise pump performance. These pumps show great potential for biomedical flow pumping, in which valveless systems are much better suited for the task, since blood damage is highly minimised in comparison with traditional turbomachinery systems. This could be a potential game changer for both extracorporeal and intracorporeal blood flow assistance. Another application is the cooling of electronic systems with valveless pumps.

Supplementary movie. A supplementary movie is available at https://doi.org/10.1017/jfm.2025.117.

Declaration of interests. The authors report no conflict of interest.

REFERENCES

ANATOL, J., GARCÍA-DÍAZ, M., BARRIOS-COLLADO, C., MONEO-FERNÁNDEZ, J.A., CASTRO-RUIZ, F. & SIERRA-PALLARES, J. 2023 Experimental characterization of an asymmetric valveless pump based on soft robotics technology. *Phys. Fluids* **35** (6), 061904.

ANATOL, J., GARCÍA-DÍAZ, M., BARRIOS-COLLADO, C., MONEO-FERNÁNDEZ, J.A., HORVATH, M., PARRA, T., CASTRO-RUIZ, F., ROCHE, E.T. & SIERRA-PALLARES, J. 2022 Experimental study of an asymmetric valveless pump to elucidate insights into strategies for pediatric extravascular flow augmentation. *Sci. Rep. UK* **12** (1), 22165.

ANATOL, J., GARCÍA-DÍAZ, M., BARRIOS-COLLADO, C., MONEO-FERNÁNDEZ, J.A., RUBIO, M., CASTRO-RUIZ, F. & SIERRA-PALLARES, J. 2024 An assessment of the suitability of a liebau pump in biomedical applications. *Phys. Fluids* **36** (1), 011908.

ANDERSSON, H., VAN DER WIJNGAART, W., NILSSON, P., ENOKSSON, P. & STEMME, G. 2001 A valve-less diffuser micropump for microfluidic analytical systems. *Sensors Actuators B: Chem.* **72** (3), 259–265.

AVRAHAMI, I. & GHARIB, M. 2008 Computational studies of resonance wave pumping in compliant tubes. *J. Fluid Mech.* **608**, 139–160.

BRINGLEY, T., CHILDRESS, S., VANDENBERGHE, N. & ZHANG, J. 2008 An experimental investigation and a simple model of a valveless pump. *Phys. Fluids* **20** (3), 033602.

DAVTYAN, R. & SARVAZYAN, N. 2021 Output of a valveless liebau pump with biologically relevant vessel properties and compression frequencies. *Sci. Rep. UK* **11** (1), 1–10.

HICKERSON, A. 2005 An experimental analysis of the characteristic behaviors of an impedance pump. *PhD thesis*, California Institute of Technology, California, USA.

HICKERSON, A., RINDERKNECHT, D. & GHARIB, M. 2005 Experimental study of the behavior of a valveless impedance pump. *Exp. Fluids* **38** (4), 534–540.

HICKERSON, A.I. & GHARIB, M. 2006 On the resonance of a pliant tube as a mechanism for valveless pumping. *J. Fluid Mech.* **555**, 141–148.

HIERMEIER, F. & MÄNNER, J. 2017 Kinking and torsion can significantly improve the efficiency of valveless pumping in periodically compressed tubular conduits. implications for understanding of the form-function relationship of embryonic heart tubes. *J. Cardiovasc. Dev. Dis.* **4** (4), 19.

JUNG, E.O. & KIM, D.W. 2012 Valveless pumping in open tank system using energy conserving compartment model. *Bull. Korean Math. Soc.* **49** (5), 961–987.

KENNER, T. 2004 Biological asymmetry and cardiovascular blood transport. *Cardiovasc. Engng* **4** (2), 209–218.

KENNER, T., MOSER, M., TANEV, I. & ONO, K. 2000 The liebau-effect or on the optimal use of energy for the circulation of blood. *Scripta Medica Facultatis Medicae Universitatis Brunensis Masarykianae* **73**, 9–14.

LEE, C.-Y., CHANG, H.-T. & WEN, C.-Y. 2008 A mems-based valveless impedance pump utilizing electromagnetic actuation. *J. Micromech. Microengng* **18** (3), 035044.

LIEBAU, G. 1954 On a valveless pump principle (ger). *Naturwissenschaften* **327**, 1.

LOUMES, L., AVRAHAMI, I. & GHARIB, M. 2008 Resonant pumping in a multilayer impedance pump. *Phys. Fluids* **20** (2), 1–12.

MANOPOULOS, C., TSANGARIS, S. & MATHIOULAKIS, D. 2020 Net flow generation in closed-loop valveless pumping. *Proc. Inst. Mech. Engrs C: J. Mech. Engng Sci.* **234** (11), 2126–2142.

MOSER, M., HUANG, J.W., SCHWARZ, GS., KENNER, T. & NOORDERGRAAF, A. 1998 Impedance defined flow generalization of william harvey's concept of circulation - 370 years later. *Intl J. Cardiovasc. Med. Sci.* **1**, 205–211.

PAHLEVAN, N. & GHARIB, M. 2013 In-vitro investigation of a potential wave pumping effect in human aorta. *J. Biomech.* **46** (13), 2122–2129.

PROPST, G. 2006 Pumping effects in models of periodically forced flow configurations. *Physica D: Nonlinear Phenom.* **217** (2), 193–201.

TAKAGI, S. & TAKAHASHI, K. 1985 Study of a piston pump without valves (2nd report). *Bull. JSME* **28** (239), 831–836.

TAKAGI, S., SAIJO, T. 1983 Study of a piston pump, without valves. *Bull. JSME* **26** (218), 1366–1372.

WEN, C.Y. & CHANG, H.T. 2009 Design and characterization of valveless impedance pumps. *J. Mech.* **25** (4), 345–354.

WEN, C.Y., CHENG, C.H., JIAN, C.N., NGUYEN, T.A., HSU, C.Y. & SU, Y.R. 2006 A valveless micro impedance pump driven by pzt actuation. *Mater. Sci. Forum* **505–507**, 127–132.

WEN, C.Y., YEH, S.J., LEONG, K.P., KUO, W.S. & LIN, H. 2013 Application of a valveless impedance pump in a liquid cooling system. *IEEE Trans. Compon. Packag. Technol.* **3** (5), 783–791.

WOMERSLEY, J.R. 1955 Method for the calculation of velocity, rate of flow and viscous drag in arteries when the pressure gradient is known. *J. Physiol.* **127** (3), 553–563.